The Search Coil Magnetometer for THEMIS

A. Roux · O. Le Contel · C. Coillot · A. Bouabdellah · B. de la Porte · D. Alison · S. Ruocco · M.C. Vassal

Received: 14 January 2008 / Accepted: 15 October 2008 / Published online: 13 November 2008 © Springer Science+Business Media B.V. 2008

Abstract THEMIS instruments incorporate a tri-axial Search Coil Magnetometer (SCM) designed to measure the magnetic components of waves associated with substorm breakup and expansion. The three search coil antennas cover the same frequency bandwidth, from 0.1 Hz to 4 kHz, in the ULF/ELF frequency range. They extend, with appropriate Noise Equivalent Magnetic Induction (NEMI) and sufficient overlap, the measurements of the flux-gate magnetometers. The NEMI of the searchcoil antennas and associated pre-amplifiers is smaller than 0.76 pT/ $\sqrt{\text{Hz}}$ at 10 Hz. The analog signals produced by the searchcoils and associated preamplifiers are digitized and processed inside the Digital Field Box (DFB) and the Instrument Data Processing Unit (IDPU), together with data from the Electric Field Instrument (EFI). Searchcoil telemetry includes waveform transmission, FFT processed data, and data from a filter bank. The frequency range covered depends on the available telemetry. The searchcoils and their three axis structures have been precisely calibrated in a calibration facility, and the calibration of the transfer function is checked on board, usually once per orbit. The tri-axial searchcoils implemented on the five THEMIS spacecraft are working nominally.

Keywords Search-coil magnetometer · Magnetospheric mission · Substorm physics

1 Introduction

The primary thrust of the Time History and Macroscale Interaction during Substorms (THEMIS) mission is to establish where and when substorms start, and to determine the nature of the instability involved in this explosive process (Angelopoulos et al. 2008;

A. Roux (ﷺ · O. Le Contel · C. Coillot · A. Bouabdellah · B. de la Porte · D. Alison · S. Ruocco Centre d'étude des Environnements Terrestre et Planétaires (CETP), 10-12 avenue de l'Europe, 78140 Vélizy, France

e-mail: alain.roux@cetp.ipsl.fr

. .

M.C. Vassal

3D Plus, 641 rue Hélène Boucher, 78532 Buc, France

url: http://www.3d-plus.com



Harvey et al. 2008). In the magnetospheric plasma, where binary collisions are almost absent, plasma waves are expected to ensure the collisionless dissipation requested by some of the substorm models, and, for guided waves, to allow a remote sensing of the dynamics of active regions. The Electric Field Instrument (EFI, see Bonnell et al. 2008 for more details) and the Search Coil Magnetometer (SCM) instruments on THEMIS are tailored to investigating the possible role played by waves at substorm breakup and during the expansion phase. THEMIS SCM has a long heritage; earlier versions of the instrument have been built for GEOS 1 and 2, Ulysses, Galileo, Interball, and more recently for Cluster, and Cassini. A description of the design for Cluster can be found in Cornilleau-Wehrlin et al. (1997, 2003). Each instrument had specific characteristics (frequency range, NEMI and weight), tailored to the constrainsts of the missions listed above. Section 2 starts with a short description of science objectives and of the requirements that they imposed on THEMIS SCM. In Sect. 3 we describe the design of THEMIS SCM antennas and preamplifiers. Section 4 provides a description of the tests and calibrations applied to the various models (one qualification, five flight models, and one spare), and compare the performances of THEMIS SCM's to the specifications. Data from SCM are digitized and processed in the Digital Fields Box (DFB) and in the Instrument Data Processing Unit (IDPU); the corresponding modes are described in the IDPU paper (Taylor et al. 2008; Cully et al. 2008). Here we simply give a short description (in Table 6) of the main characteristics of various operation modes.

2 Measurement Requirements

2.1 Science Objectives

There are basically two types of models for substorm breakup (see for instance Lui 2001 and references therein). For the first type of model, magnetic reconnection (MR) occurs first and triggers substorms. In the second type of model, labelled "Current Disruption" (CD), the breakup is triggered by a reduction in the cross-tail current, associated with the development of an instability. In both cases ULF and ELF waves are believed to play a critical role. In the MR models whistler mode waves are expected to accelerate electrons up to large (super-Alfvénic) velocities (Mandt et al. 1994). Very thin current sheets can also be destabilized by HF tearings in the whistler mode (Bulanov et al. 1992). In CD models the cross tail current is disrupted by HF cross field instability (Lui et al. 1992), or undergo LF (ballooning modes) instabilities (Roux et al. 1991) which are coupled to higher frequency waves: ion cyclotron, lower hybrid drift and/or whistler modes. Thus wave observations provide a critical test to substorm scenarios. THEMIS SCM, and EFI (which measure electric fields in the same frequency range) are designed to identify waves associated with the breakup and to investigate their role in substorm dynamics. Furthermore, when the waves are guided, they can be used to help remotely track the active region where breakup starts. SCM is also needed to assess the nature of the waves; are they electrostatic (such as lower hybrid waves), or electromagnetic (such as whistler mode waves)?

2.2 Requirements

2.2.1 Frequency Range and NEMI

The science objectives briefly sketched above, and described in more details in a companion paper by Le Contel et al. (2008), have been used to specify the characteristics of THEMIS



SCM. We summarize the main instrument requirements below. Among the various types of wave modes listed above, whistler mode waves have the highest frequency cut-off: f_{ce} (the electron gyrofrequency), in the regions of interest. This cut-off has been used to fix the maximum frequency to be covered by the SCM. CD is expected to develop in the nearearth plasma sheet, typically around 8 $R_{\rm E}$ (Lui et al. 1992). At 8 $R_{\rm E}$, $B \simeq 50$ nT is a typical value for the DC field, then $f_{ce} \simeq 1.4$ kHz. At the geostationary orbit (6.7 $R_{\rm E}$), assuming a dipole field, one gets $f_{ce} \simeq 4$ kHz, while during a substorm growth phase, where the average equatorial magnetic field is reduced by the effect of the increasing cross tail current, one gets $f_{ce} \simeq 2.8$ kHz. At 5 $R_{\rm E}$, the dipole field gives $f_{ce} \simeq 9$ kHz, which is about twice the maximum frequency covered by the SCM instrument. Since CD is not expected to occur inside of 5–6 $R_{\rm E}$, and whistler mode waves are damped and/or unguided above $f_{ce}/2$, an upper cutoff of the SCM frequency bandwith at 4 kHz has been imposed. Given that the amplitude of waves measured in the plasma sheet by Cluster is typically on the order of 10–100 pT/ $\sqrt{\rm Hz}$ at 10 Hz, the requirement for SCM NEMI is to be better than 1 pT/ $\sqrt{\rm Hz}$ at 10 Hz.

2.2.2 Other Requirements

Given the constrainsts on spacecraft mass, the allocated mass budget was 800 g (600 g for the sensors, including mounting hardware, and 200 g for the preamplifiers), while the power allocation was fixed to be smaller than 100 mW, for each set of SCM preamplifiers (Harvey et al. 2008). In order to determine the polarization of the waves, the direction of the magnetic axis of the antennas has to be known. Thus the direction of each antenna axis has to be known to better than 1 degree. In Sect. 3 we show that these requirements are met by the five tri-axis SCMs deployed on THEMIS.

3 Description of the Instrument

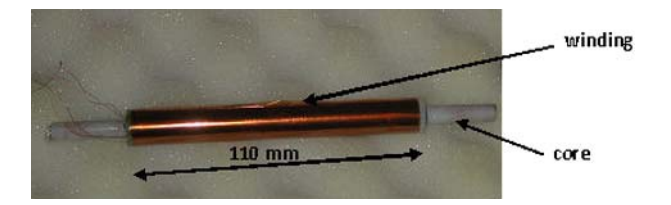
3.1 Modeling

3.1.1 Magnetic Amplification

The instrument is based upon the combination of a high magnetic permeability material and a large number of turns which passively detect voltage induced by the changing external field (an AC-current measurement). The high magnetic permeability core amplifies the external magnetic field (Ripka 2001; Osborn 1945; Bozorth and Chapin 1942; Coillot et al. 2007). This core is located inside two types of windings. The main winding is the sensing element; it has a very large number of turns; 51 600 in our case, while the secondary winding is used to introduce a flux feedback in order to flatten the frequency response by removing the resonance associated with the main winding. The flux feedback stabilizes the phase response of the instrument, independent of temperature variations. Figure 1 shows a picture of a search coil before potting. The magnetic amplification, or apparent permeability μ_{app} , characterizes the ratio between the magnetic field at a given position in the core B_{core} , and the external magnetic field B_{ext} . In practice one must define a mean apparent permeability that describes the average field seen inside a winding of length L. The main winding has N turns wound around a core with a relative permeability μ_r . In these conditions, Lenz's law



Fig. 1 Picture of a THEMIS search coil before potting



 $e = -Nd/dt(\phi)$, where ϕ is the magnetic flux across one loop, gives the modulus of the induced voltage as

$$e = NS\left(\frac{1}{L}\int_{0}^{L}\mu_{app}(l)dl\right)B_{ext}\omega = NS < \mu_{app} > B_{ext}\omega. \tag{1}$$

S is the core section, assuming a sinusoidal magnetic perturbation ($B_{ext} \propto \exp(j\omega t)$) and the brackets denote an averaging along the winding. When a magnetic field is applied to ferromagnetic materials, they become magnetized. The intensity of this magnetization depends on the relative permeability of the magnetic material, and the shape of the sample via its demagnetizing coefficient N_z . The latter depends on the ratio m between the length and the diameter of the magnetic core. In the case of a cylinder we utilize the expression:

$$\mu_{app}(m) = \frac{B_{core}}{B_{ext}} = \frac{\mu_r}{[1 + (\mu_r - 1)Nz(m)]}.$$
 (2)

For the magnetic material used for THEMIS, the relative permeability is very high, thus $(\mu_r - 1)Nz(m) \gg 1$ and the previous expression becomes: $\mu_{app}(m) = 1/Nz(m)$. Then, in order to increase the apparent permeability, one must decrease the coefficient of the demagnetizing field, increasing the ratio m. This can be done either by increasing the length L or decreasing the diameter d. In the first case, the size and mass of the sensor is increased, and in the second the intensity of the induced voltage is reduced, since the section of the core is decreased. The design of the THEMIS search coil results from a compromise between these two constrainsts; the dimensions of the magnetic core are: L = 170 mm and d = 7 mm, see Fig. 1.

3.1.2 Electrical Modeling

The frequency behaviour can be represented by an RLC circuit excited by a voltage source corresponding to the induced voltage collected by the main winding, as shown in Fig. 2. The transmittance (ratio between the output voltage V and the measured magnetic field B) of such a sensor can be easily put in the following form:

$$T(j\omega) = \frac{V}{B} = \frac{-j\omega N S \mu_{app}}{(1 - LC\omega^2) + jRC\omega}.$$
 (3)

The sensor has a main resonance which limits its measurement bandwidth and reduces the dynamics. This is because a signal measured at a frequency close to the resonant frequency leads to a high transmittance value. To remove this effect, the output of the high gain preamplifier (from the primary winding) is used to generate a feedback flux inside the core via the secondary winding as shown in Fig. 3. In other words the feedback current flowing through the secondary winding (via a feedback resistor) generates a magnetic field along the search-coil axis proportional to the external magnetic field but in the opposite direction. Therefore



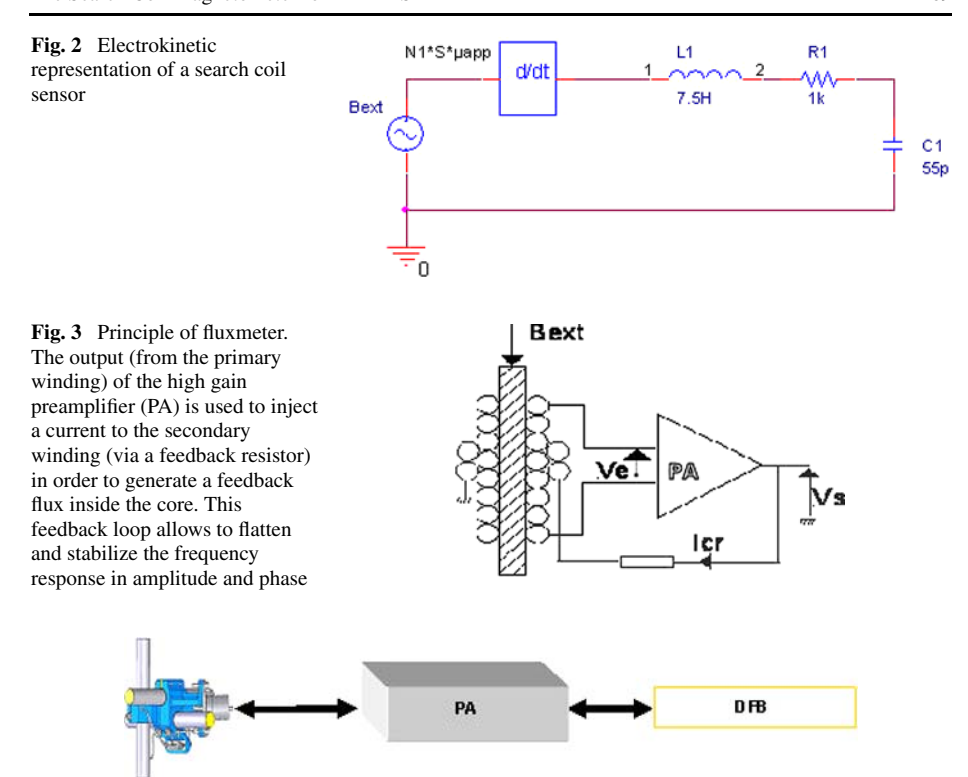


Fig. 4 Block diagram: the three analog signals are amplified by the preamplifier (PA) and then digitized by the digital field box (DFB)

this feedback flux, which is proportional to the flux generated by the external magnetic field, allows to flatten and stabilize the frequency response of the antenna. The value of the feedback resistor controls the strength of the feedback. The smaller the value of the resistor, the stronger the feedback is.

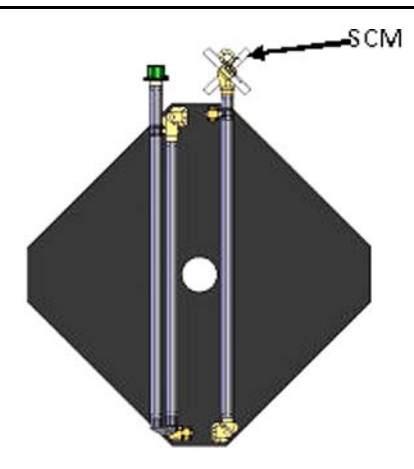
3.2 Design of THEMIS SCM

3.2.1 SCM Antennas

The Search Coil Magnetometer consists of three sensors and a preamplifier box connected to the DFB (Digital Field Board) as shown in Fig. 4. The sensors are mounted in a tri-axial configuration to measure the x, y, and z components of the magnetic field in the frequency range of 0.1 Hz–4 kHz. They are mounted on the tip of a one meter length rigid boom as shown in Fig. 5 (stowed position). Such a boom length allows for a reduction of the level of the electromagnetic noise coming from the spacecraft and detected by the antennas (Ludlam et al. 2008). The deployed configuration is displayed in a companion paper (Le Contel et al. 2008) and the axis definitions are described. The antenna structure is designed to allow a precise alignment of the sensors with respect to the spacecraft axis. Two sensors lie in the spin plane and the third one is parallel to the spin axis. The 3 SCM antennas are held orthogonally on a mechanical structure mounted on a one-probe diameter boom; they are thermally isolated and covered by a thermal blanket of Multi-Layer Insulation (MLI).



Fig. 5 SCM position on the probe (drawing from UCB)



The identical sensor (18 cm) and its kin (27 cm) have been previously flown by CETP on more than 7 earth-orbiting and interplanetary missions; most-recently it was flown as part of the Cluster/STAFF experiment. The mass of the SCM antennas and mounting structure is 568 g, compliant with THEMIS specifications (less than 600 g). Electrostatic shielding is implemented around the search coils to minimize their sensitivity to electric fields.

3.2.2 Preamplifier Design

Three identical low-power preamplifiers (one for each sensor signal) are mounted in an electrical unit, fixed on the IDPU box (Taylor et al. 2008). They have been developed using a new technology: multichip module vertical (MCM-V). The MCM-V technology allows a significant reduction in the mass and the volume of the preamplifiers. It is also well adapted to withstand a severe radiation environment. This technique consists of dividing the circuit in smaller functions. Each function is implemented using bare chips on thin flexible printed circuit boards (PCB), which are piled up to form a compact module (essentially a cube, see Fig. 6). Layers containing tantalum plates are inserted between the PCBs to protect the sensitive components against radiation. These plates are placed only on the top and bottom of these sensitive components. This spot shielding has the advantage of being lighter than more traditional techniques. These preamplifiers have low-noise input stages. Their dynamic range is about 100 dB, which allows weak signals to be measured in the presence of the large voltage signals induced by the rotation of the spacecraft in the DC magnetic field. They benefit from a specific power supply which is also realized in MCM-V technology and corresponds to a fourth cube. A specific SCM calibration signal is generated inside the preamplifier box. The use of this calibration is discussed in the next section. The mass and power consumption of SCM preamplifier are 200 g and 75 mW, respectively, which is compliant with specifications.

4 Calibrations and Tests

The experiment transfer function and NEMI are given in Figs. 7 and 8; they were measured on the ground in a calibration facility, at Chambon la Forêt, France. The NEMI of each flight model is shown in Tables 1 to 5. The largest NEMI is $0.76 \, \text{pT}/\sqrt{\text{Hz}}$ at 10 Hz which complies





Fig. 6 Preamplifier box. The 3 upper cubes correspond to the 3 antennas preamplifiers, the fourth one is for power regulation. They are manufactured in 3D technology. The electronics for the in-flight calibration is also shown on the PCB. The preamplifier box size is $95 \text{ mm} \times 81 \text{ mm}$ (109 with the mounting "ears") \times 30 mm. The mass is 200 g

Fig. 7 Frequency response (transfer function) of the SCM with feedback (*blue*) and without (*pink*)

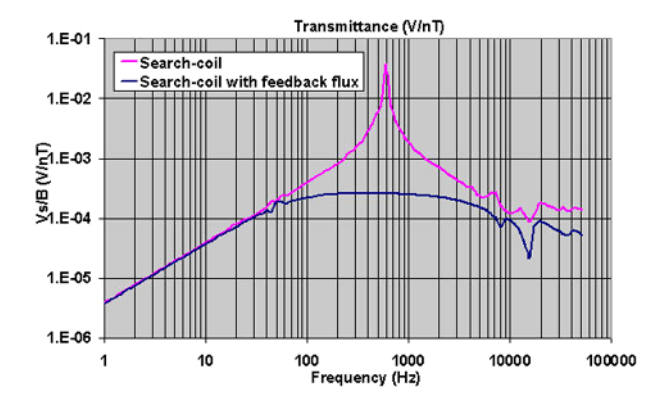




Fig. 8 Transfer function (*pink*) in dB V/nT and NEMI (in *blue*) in nT/ $\sqrt{\text{Hz}}$ of THEMIS search coil measured in the calibration facility at Chambon la Forêt

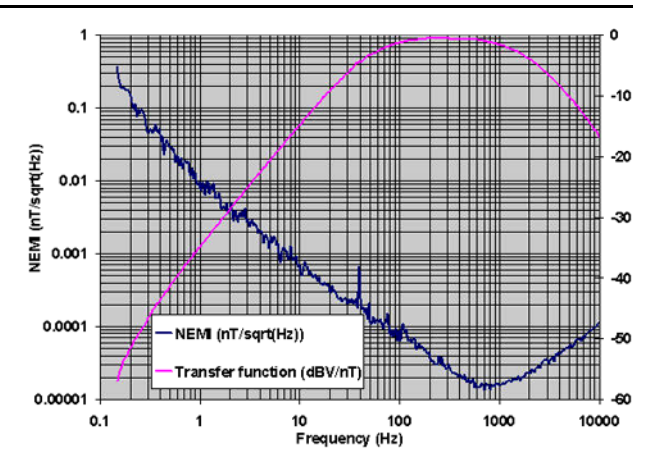


Table 1 NEMI of FM1

FM1	10 Hz	100 Hz	1 kHz
X	0.69	0.070	0.022
Y	0.65	0.072	0.021
Z	0.64	0.077	0.021

Table 2 NEMI of FM2

FM2	10 Hz	100 Hz	1 kHz
X	0.64	0.0699	0.020
Y	0.65	0.0698	0.020
Z	0.645	0.076	0.022

Table 3 NEMI of FM3

FM3	10 Hz	100 Hz	1 kHz
X	0.61	0.070	0.0196
Y	0.66	0.067	0.016
Z	0.74	0.066	0.019

Table 4 NEMI of FM4

FM4	10 Hz	100 Hz	1 kHz
X	0.71	0.079	0.017
Y	0.76	0.08	0.019
Z	0.74	0.077	0.019

with the specified value (1 pT/ $\sqrt{\text{Hz}}$). At 100 Hz the largest NEMI is 0.08 pT/ $\sqrt{\text{Hz}}$, and at 1 kHz it is 0.022 pT/ $\sqrt{\text{Hz}}$.

It can be seen that they are quite close. The transfer functions are also almost identical, with less than 1 dB difference between the models. In order to determine the polarization of the waves on each satellite and to accurately compare data from the five satellites, careful measurements of the angle between each magnetic axis and its corresponding mechanical



Table 5 NEMI of FM5	FM5	10 Hz	100 Hz	1 kHz
	X	0.66	0.065	0.016
	Y	0.70	0.074	0.016
	Z	0.72	0.069	0.016

Table 6 Telemetry modes for SCM

APID	Processing	Characteristics and comments
440	Filter bank (fbk)	Mean value of the signal in 6 frequency bands kHz: [4–2]; [1–0.5]; Hz: [256–128]; [64–32]; [16–8]; [4–2] Sampling rate: 1/16 to 8 S/s There are only 2 inputs to be shared within 3 SCM and 12 EFI components
444	Fast survey (scf)	Waveform data for the 3 SCM components Sampling rate within 2 to 256 S/s, nominal value is 8
448	Particle burst (scp)	as 444 but nominal value is 128 S/s
44C	Wave burst (scw)	as 444 but nominal value is 8192 S/s
44D	Particle burst spectra (ffp)	Compressed FFT with 16, 32 or 64 frequency lines, nominal value is 32
		Sampling rate from 1/4 to 8 Spectra/s, nominal value is 1
		There are only 4 inputs to be shared within 20 possible signals including the 3 SCM components
44E	Wave burst spectra (ffw)	as 44D but nominal values are 64 frequency lines and 8 Spectra/s

axis have been made. These angles may be just a few degrees, but need to be known with precision. The estimated error in the knowledge of the magnetic axis is 0.5 degrees which is less than the 1 degree in specifications. For example the angle of sensor X of the flight model 3 (FM3) is 0.2 degrees. For each sensor the angle difference between mechanical and magnetic axes can be neglected. Thus the magnetic field can be accurately transformed into any required reference frame. A free running onboard oscillator generates a 9 Hz triangular wave used to check the transfer function inflight. A digital command is activated by the DFB (Cully et al. 2008) to connect this signal to the feedback winding of the sensors. This signal is detected by the primary winding, and seen in B_x , B_y , and B_z data. The default duration is 30 seconds with a maximum of 60 seconds. This signal contains many frequencies throughout the bandwidth, which are used for in flight calibration.

Further signal processing takes place inside the IDPU, on a single board, together with the EFI instrument. The analog signals output by SCM are filtered, sampled, and converted to digital in the DFB and the IDPU. Taking into account that SCM measurements are digitized with 16 bits and that it must comply with the NEMI requirements, the SCM measurement is likely to saturate for an AC magnetic field about 1000 nT. The spin of the spacecraft will cause the DC magnetic field to saturate the SCM at the spin frequency, at altitudes less than approximately 4 $R_{\rm E}$. The different modes of data transmission are listed in Table 6 and described in the IDPU and DFB papers (Taylor et al. 2008; Cully et al. 2008). SCM data is transmitted in the following modes: Fast Survey (Application Identifier or APID number



444) at sampling rates between 2 Hz and 256 Hz, Particle Burst (APID 448) at 2–256 Hz, Wave Burst (APID 44C) at 512 Hz to 8 kHz, Spectra (APID 44D and 4E), and Filter Banks (APID 440) where the power in six frequency bands is calculated: 2–4 kHz, 0.5–1 kHz, 128–256 Hz, 32–64 Hz, 8–16 Hz, and 2–4 Hz (see Table 6 for more details).

5 Summary and Conclusions

The SCM instruments implemented on the five THEMIS probes measure the 3D magnetic field fluctuations in the frequency bandwidth from 0.1 Hz to 4 kHz. The weight and power consumption comply with THEMIS requirements. They extend with appropriate NEMI and sufficient overlap, the measurements of the FGM beyond the 1 Hz range. We have described the design of THEMIS SCM. Tests and calibrations carried out in a calibration facility, at Chambon la Forêt, demonstrate that the five sets of triaxial search coils cover the same frequency range, have the same frequency response, and the same NEMI. SCM instruments fulfill all mission requirements. The NEMI at 10 Hz is smaller than 0.76 pT/ $\sqrt{\text{Hz}}$ for each instrument while the NEMI at 1 kHz is about 20 fT/ $\sqrt{\text{Hz}}$. Onboard calibration is usually performed once per orbit in order to check the stability of the transfer function. The magnetic axes are known to better than 1 degree; as requested. The 0.1 Hz to 4 kHz frequency range is covered by EFI and SCM, in the same manner. SCM and EFI data are filtered, processed and transmitted to the ground via THEMIS DFB/IDPU. The tri-axes SCMs, on each of the five THEMIS spacecraft, are working nominally.

Acknowledgements The French involvment on THEMIS is supported by CNES and CNRS. Vacuum tests and integrations of the SCM were made at UCB. We are pleased to acknowledge the friendly collaboration and the help of our colleagues at UCB, in particular V. Angelopoulos, P. Harvey, R. Jackson, M. Ludlam, D. Meilhan, H. Richard, and E. Taylor. Work in the US was supported by NASA contract NAS5-02099.

References

- V. Angelopoulos et al., The THEMIS mission. Space Sci. Rev. (2008, this issue). doi:10.1007/s11214-008-9336-1
- J.W. Bonnell, F.S. Mozer, G.T. Delory, A.J. Hull, R.E. Ergun, C.M. Cully, V. Angelopoulos, The electric field instrument (EFI) for THEMIS. Space Sci. Rev. (2008, this issue)
- R.M. Bozorth, D.M. Chapin, Demagnetizing factors of rods. J. Appl. Phys. 13, 320–326 (1942)
- S.V. Bulanov, F. Pegoraro, A.S. Sakharov, Magnetic reconnection in electron dynamics. Phys. Fluids B 4, 2499–2508 (1992)
- C. Coillot, J. Moutoussamy, P. Leroy, G. Chanteur, A. Roux, Improvements on the design of search coil magnetometer for space experiments. Sens. Lett. 5, 1–4 (2007)
- N. Cornilleau-Wehrlin, P. Chauveau, S. Louis, A. Meyer, J. Nappa, S. Perraut, L. Rezeau, P. Robert, A. Roux, C. de Villedary, Y. de Conchy, L. Friel, C.C. Harvey, D. Hubert, C. Lacombe, R. Manning, F. Wouters, F. Lefeuvre, M. Parrot, J.L. Pinçon, B. Poirier, W. Kofman, P. Louarn, The cluster Spatio-temporal Analysis of Field Fluctuations (STAFF) experiment. Space Sci. Rev. 79, 107–136 (1997)
- N. Cornilleau-Wehrlin, G. Chanteur, S. Perraut, L. Rezeau, P. Robert, A. Roux, C. de Villedary, P. Canu, M. Maksimovic, Y. de Conchy, D. Hubert, C. Lacombe, F. Lefeuvre, M. Parrot, J.-L. Pinçon, P.M.E. Décréau, C.C. Harvey, P. Louarn, O. Santolik, H.St. Alleyne, M. Roth, T. Chust, O. Le Contel, STAFF team, First results obtained by the Cluster STAFF experiment. Ann. Geophys. 21, 437–456 (2003)
- C.M. Cully, R.E. Ergun, K. Stevens, A. Nammari, J. Westfall, The THEMIS digital fields board. Space Sci. Rev. (2008, this issue). doi:10.1007/s11214-008-9417-1
- P.R. Harvey et al., The THEMIS observatory. Space Sci. Rev. (2008, this issue)
- O. Le Contel, A. Roux, P. Robert, C. Coillot, A. Bouabdellah, B. de la Porte, D. Alison, S. Ruocco, V. Angelopoulos, K. Bromund, C.C. Chaston, C. Cully, First results of THEMIS Search Coil Magnetometers (SCM). Space Sci. Rev. (2008, this issue). doi:10.1007/s11214-008-9371-y



- M. Ludlam et al., The THEMIS magnetic cleanliness program. Space Sci. Rev. (2008, this issue). doi:10. 1007/s11214-008-9423-3
- A.T.Y. Lui, Current controversies in magnetospheric physics. Rev. Geophys. **39**(4), 535–563 (2001)
- A.T.Y. Lui, R.E. Lopez, B.J. Anderson, K. Takahashi, L.J. Zanetti, R.W. McEntire, T.A. Potemra, D.M. Klumpar, E.M. Greene, R. Strangeway, Current disruption in the near-Earth neutral sheet region. J. Geophys. Res. 97, 1461 (1992)
- M.E. Mandt, R.E. Denton, J.F. Drake, Transition to whistler mediated magnetic reconnection. Geophys. Res. Lett. 21(1), 73–77 (1994)
- J.A. Osborn, Demagnetizing factors of the general ellipsoid. Phys. Rev. 67(11–12), 351–357 (1945)
- P. Ripka, Magnetic sensors and magnetometers. Artech house (2001)
- A. Roux, S. Perraut, P. Robert, A. Morane, A. Pedersen, A. Korth, G. Kremser, B. Aparicio, D. Rodgers, R. Pellinen, Plasma sheet instability related to the westward traveling surge. J. Geophys. Res. 96, 17,697 (1991)
- E. Taylor et al., The THEMIS instrument data processing unit. Space Sci. Rev. (2008, this issue)

